

Article

Residence Time Distribution Analysis of Drip-Irrigated Beds—The Effect of Material and Fluid Properties with Implications for Heap Leaching Practice

Michael D. Odidi ^{1,2}, Marijke A. Fagan-Endres ^{1,*} and Susan T. L. Harrison ¹

¹ Centre for Bioprocess Engineering Research, Department of Chemical Engineering, University of Cape Town, Cape Town 7700, South Africa

² Mintek, Randburg 2125, South Africa

* Correspondence: marijke.fagan-endres@uct.ac.za

Abstract: The quantitative effect of particle shape, porosity, wettability, particle size, and solution viscosity on the residence time distribution (RTD) profiles of non-reactive, steady-state, drip-irrigated ore beds characteristic of heap leaching systems is presented. Results were obtained using step-up tracer tests and allowed for the analysis of preferential flow behaviour within the systems. The key findings were as follows. Increased particle sphericity enhanced channelling in beds of smaller particles, but not for larger particle sizes. Higher particle wettability caused greater liquid dispersion during both initial wetting studies and at steady-state fluid flux. Higher porosity levels and the inclusion of fines in mixed sized beds resulted in longer average solute residence times, higher liquid hold-up, longer solution and tracer breakthrough times, and increases in drain-down moisture percentages. Increasing the irrigation fluid's viscosity, reflective of the increase in ionic concentrations in leach solutions, reduced both the solution and tracer breakthrough times and increased dispersion with signs of more discontinuous or isolated fluid volumes at steady-state. These results highlighted the importance of the inclusion of fines in agglomerated beds to improve uniform wetting especially those with low to moderate particle porosities (<2.5 m²/g specific surface area). The viscosity results suggest that there may be changes in preferential flow extent, due to variations in viscosity owing to the increasing sulphate concentration within the liquid phase in heaps and with time.

Keywords: preferential flow; heap leaching; capillary action; particle size; porosity; wettability; viscosity



Citation: Odidi, M.D.; Fagan-Endres, M.A.; Harrison, S.T.L. Residence Time Distribution Analysis of Drip-Irrigated Beds—The Effect of Material and Fluid Properties with Implications for Heap Leaching Practice. *Minerals* **2023**, *13*, 267. <https://doi.org/10.3390/min13020267>

Academic Editor: Fang Xia

Received: 5 December 2022

Revised: 23 January 2023

Accepted: 8 February 2023

Published: 14 February 2023



Copyright: © 2023 by the authors. Licensee MDPI, Basel, Switzerland. This article is an open access article distributed under the terms and conditions of the Creative Commons Attribution (CC BY) license (<https://creativecommons.org/licenses/by/4.0/>).

1. Introduction

The use of residence time distribution (RTD) data in the analysis of solute transport and fluid flow profiles within irrigated packed beds has been extensively studied in trickle bed reactors. These systems are typically composed of uniform, well characterised packings or catalysts with defined porosities and geometries [1]. However, the data obtained from such uniform beds cannot be readily applied to more complex systems such as those typically encountered during the leaching of low-grade mineral ores or agglomerated concentrates applied commercially as heap leaching and investigated more fundamentally in laboratory and pilot test work through column studies [2,3]. In the latter, irregularly shaped crushed ore particles or representative materials with a distribution of particle sizes are loaded into a column to simulate geometric cross-sections of heaps. Such column tests are mainly used to demonstrate feasibility and obtain bulk kinetic data related to the chemistry, microbiology, and hydrodynamics of the leaching system being studied [3] as well as data on the extent of reaction achieved. The data obtained are useful for scale-up operations. To supplement this, further data are required to develop strategies to further optimize the heap leaching process. Examples include avoidance of preferential flow, insurance of lateral fluid motion to fully wet the heap, and balancing of the particle size used to ensure liberation, appropriate fluid flow, and contacting.

Preferential flow is related to the hydrodynamics of a heap and reveals itself on two different scales, illustrated in Figure 1. At the bed scale, preferential flow is defined as the uneven distribution of drip-irrigated solution within an ore bed resulting in dry sections that do not encounter the irrigation fluid. At the solution scale, which focuses on the wetted sections of the bed, the division of the liquid volume into actively flowing channels and stagnant or slow-moving solution pools is a further manifestation of preferential flow [4]. Preferential flow has been linked to less than expected metal extraction rates and, in extreme cases, heap failures [5,6]. Therefore, studies of the hydrodynamic behaviour of irrigated ore beds are beneficial and necessary for the improvement of heap design and practice. Previous research in this area has dealt with aspects such as the effect of particle size distribution [7,8], material shape [9,10], material porosity [11], packing arrangement [12,13], segregation [14], hysteresis [15,16], bed scale [17,18], and irrigation rate [9,16,19,20] on heap hydrodynamics.

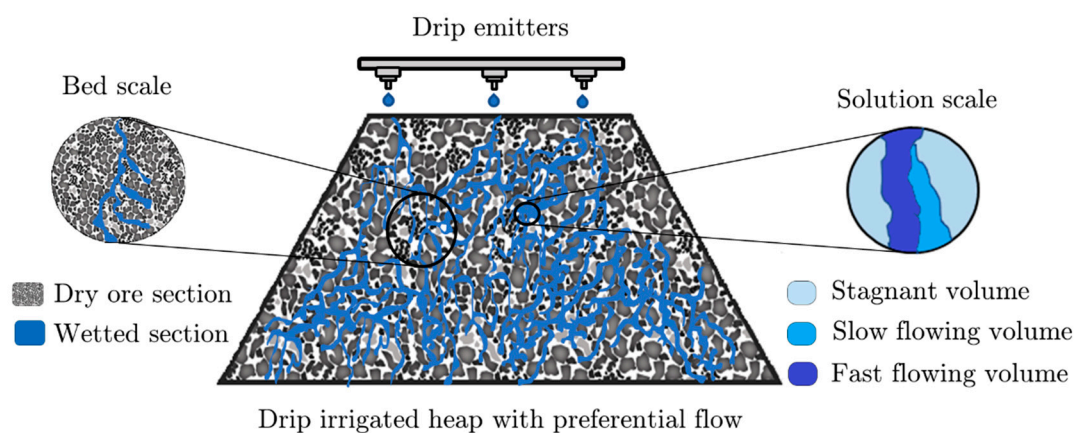


Figure 1. Preferential flow depiction on two scales in a drip-irrigated heap.

Though the abovementioned studies have contributed to the current knowledge base significantly, areas requiring further research still exist. Studies focusing on transient liquid hold-up behaviour are beneficial in elucidating the effects of irrigation rate and hysteresis on bed scale preferential flow [11,15,16]. However, they have limited ability to accurately diagnose the presence of stagnant and isolated solution volumes. In such cases, drain-down data are relied upon to obtain the fraction of actively flowing solution, but their accuracy is largely dependent on the allocated drainage time [7,11]. RTD studies provide a more detailed analysis on the level of accessibility of solution volumes to solute molecules within a packed bed.

Hydrodynamic data generated using spherical glass beads as non-porous alternatives to ore particles or other materials in packed beds [21] have been used to quantify the effect of particle porosity on the flow characteristics in irrigated columns [11,22–24]. However, this has led to the need for the decoupling of the effect of particle porosity from that of particle shape on hydrodynamic data in laboratory leaching tests to elucidate critical factors in the heap. The effect of the intrinsic wettability of packing materials has also been neglected. With regards to particle size distribution, previous studies have varied the top particle size [7] or investigated narrow and broad size ranges in isolated or segregated systems [6,8,13,23,25], but the effect of fines (defined in this paper as <1 mm particles) and the culminative effect of narrow particle size fractions within mixed size beds has not been fully investigated under conditions typical of a heap. Lastly, the effect of variations in irrigation fluid viscosity on the RTD data and associated parameters have not been considered in a heap leaching context. This is despite previous studies having utilised a variety of irrigation fluids with varying compositions and hence viscosities, based on theoretical and empirical viscosity models [26], with sulphate ions known to have an effect on solution viscosity [27].

This study addresses the four gaps mentioned above through the generation of steady-state RTD data obtained from salt tracer tests conducted on packed beds composed of different materials with defined inherent properties and size distributions. The selected materials and size distributions aid in decoupling the effects of particle shape from particle porosity, whilst allowing for the effects of particle wettability on the generated RTD profiles to be elucidated. The effect of irrigation fluid viscosity is studied using a viscosity modifier. The data obtained are used in the quantification of relevant RTD parameters, which are analysed, compared, and discussed for a better understanding of the factors affecting fluid distribution in steady-state drip-irrigated packed beds.

2. Experimental

2.1. Solid Material Selection and Characterisation

Four different solid materials were selected for use, with unique inherent properties relevant to leaching studies: glass beads (GBs), glass shards (GSs), greywacke (GW), and malachite ore (MO) (refer to Figure 2). The GBs (Figure 2a) were purchased from Sigma Aldrich and Lasec. The GSs (Figure 2b) were obtained from piles of broken ‘windscreen’ glass at a PG Glass centre located in Cape Town, South Africa. The GW stones (Figure 2c) were purchased from an AfriSam plant, a supplier of construction materials, also located in Cape Town. GW is classified as a sedimentary rock consisting mainly of quartz and feldspar. The GSs and GW stones were crushed using a jaw crusher, pulverized, and sieved into different size fractions in the Mineralogy Laboratory at the University of Cape Town (UCT). Mintek (Randburg, South Africa) provided the crushed, split, and sieved MO samples (Figure 2d) which were further sieved into more sized fractions prior to their analysis and use.

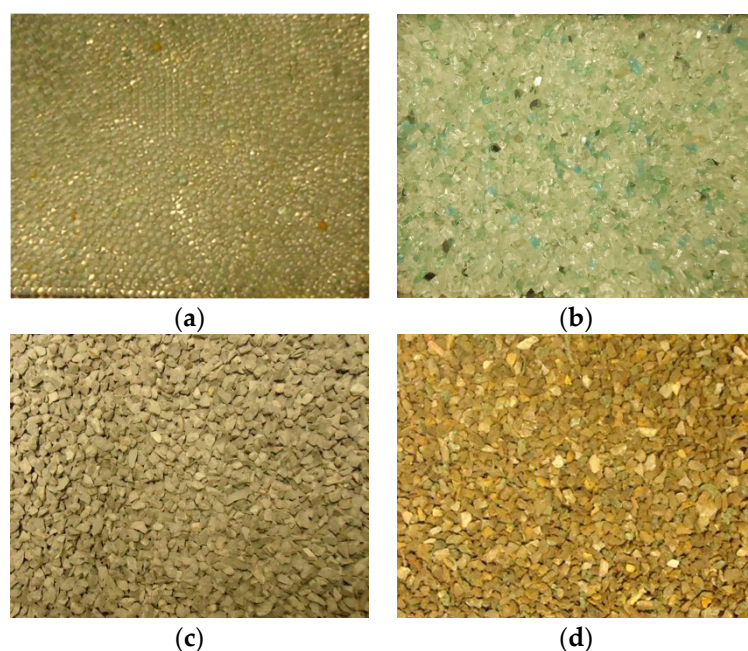


Figure 2. Photographs of the different packing materials: (a) glass beads (GB: 2 mm), (b) glass shards (GS: 4.8–5.6 mm), (c) greywacke (GW: 4.8–5.6 mm), and (d) malachite ore (MO: 4.8–5.6 mm).

Brunauer–Emmett–Teller (BET) analysis on the porous materials (GW and MO) was conducted at the UCT Chemical Engineering Analytical Laboratory. The Micrometrics TriStar II 3020 Surface Area and Porosity instrument at a bath temperature of $-195.8\text{ }^{\circ}\text{C}$ was used to obtain the average specific pore area of the materials. Based on the results in Table 1 and comparative data of a group of sulphide minerals from a study by Xia et al. [28] shown in Table 2, the MO sample was classified as highly porous compared to the moderately porous GW particles. The GSs and GBs were assumed to be non-porous.

Table 1. BET analysis results for greywacke and malachite ore.

Material	Size Fraction (mm)	BET Surface Area (m ² /g)
Greywacke	0.1–0.5	1.68 ± 0.01
	0.5–1.0	1.01 ± 0.01
Malachite ore	0.1–0.5	5.88 ± 0.05
	0.5–1.0	2.58 ± 0.02

Table 2. Specific surface area of sulphide minerals using small-angle neutron scattering (SANS) and ultra-small-angle neutron scattering (USANS) [28].

Material	Size (µm)	Surface Area (m ² /g)
Violarite	20–53	3.36
Marcasite	20–53	0.94
Pyrite	20–53	3.56
Bornite	20–53	0.99
Chalcopyrite	20–53	2.73

Wettability measurements on the irregularly shaped materials (GSs, GW, and MO) were carried out using a Krüss force tensiometer (K12/MK4 from Advanced Laboratory Solutions). Prior to analysis, the materials were pulverised to a size fraction of 0.038–0.053 mm and loaded into a miniature glass column. The Washburn equation along with the upward infiltration capillary suction method were used to calculate the contact angles. The results in Table 3 show that the materials could be grouped in order of decreasing wettability as GW > GSs > MO.

Table 3. Average contact angles obtained from wettability experiments conducted on three selected materials using different solutions at 30 °C.

Material	Liquid	Contact Angle
Glass shards (GS)	Water	49.9 ± 3.3
Greywacke (GW)	Water	40.1 ± 2.9
	Water	62.9 ± 3.4
Malachite ore (MO)	15 wt% Glycerol	64.4 ± 0.9
	25 wt% Glycerol	63.0 ± 0.5
	30 wt% Glycerol	63.0 ± 0.5
	35 wt% Glycerol	63.6 ± 0.5

The only leachable material, MO, was analysed by quantitative evaluation of minerals by scanning electron microscopy (QEMSCAN) at UCT and found to contain mainly quartz (76.8%), malachite (6.8 wt%), ilmenite (4.5 wt%), muscovite (3.6 wt%), and bornite (2.4 wt%). The other materials were not analysed as they had more defined compositions.

Two-dimensional shape characterisation was carried out on the different materials in the size range of 1 to 8 mm. The particles were arranged on a light box in a grid-like pattern. A Sony Cyber-shot DSC-W530 14.1 mega-pixel digital camera was then used to capture images of the arranged particles. The particles for both the GBs and GSs were spray-painted matte black to maximise the contrast with their background. Three hundred particles per specific narrow size fraction within the 1 to 8 mm range were analysed for the GSs, GW, and MO materials. Ten beads per discrete size class (2 and 5 mm) were analysed for the GBs. The images were processed using the BioVoxel Toolbox plugin which is part of the ImageJ computer software program. Part of the analysis involved the quantification of five 2D shape descriptors found in Table 4. The results indicate that the GBs were the closest

in shape to a perfect sphere while there were no substantial differences in the average shape descriptor values obtained for the other three materials. A summary of the relevant physical properties of the selected materials can be found in Table 5.

Table 4. Average and standard deviation shape descriptor values obtained for the 2 and 5 mm glass beads (GBs) and over the 1–8 mm size fraction range for the glass shards (GSs), greywacke (GW), and malachite ore (MO) materials. The values are compared to those calculated for a perfect sphere (PS).

Shape Descriptor	Calculated Value	Average Values			
	PS	GB	GS	GW	MO
Aspect ratio	1.00	1.05 ± 0.01	1.55 ± 0.44	1.62 ± 0.45	1.58 ± 0.41
Circularity	1.00	0.88 ± 0.00	0.74 ± 0.08	0.73 ± 0.08	0.72 ± 0.08
Compactness	1.00	0.98 ± 0.01	0.82 ± 0.09	0.81 ± 0.09	0.81 ± 0.09
Extent	0.79	0.77 ± 0.01	0.68 ± 0.09	0.67 ± 0.07	0.67 ± 0.07
Solidity	1.00	0.97 ± 0.01	0.94 ± 0.03	0.93 ± 0.03	0.92 ± 0.03

Table 5. Summary of the physical properties of the selected materials.

Property	Packing Material			
	GB	GS	GW	MO
Composition	Uniform	Uniform	Non-uniform	Non-uniform
Porosity	Non-porous	Non-porous	Porous	Highly porous
Shape	Spherical	Irregular	Irregular	Irregular
Packing Orientation	Ordered	Random	Random	Random
Wettability	Moderate	Moderate	High	Low

2.2. Liquid Characterisation

A Cannon–Fenske glass capillary viscometer was used to measure the viscosity of five glycerol (viscosity modifier) solutions with viscosities ranging from 0.8 to 2.2 cP. This covered both the lower (0.8 cP for a 0 g/L SO_4^{2-} solution at 30 °C, data not shown) and upper (1.45 cP for a 100 g/L SO_4^{2-} solution at 30 °C, data not shown) range encountered in heap leaching laboratory test work investigating the effect of sulphate ion concentration in leaching systems [27]. Gravimetric analysis was used to acquire density values for the test solutions. All of the measurements were conducted at 30 °C. The solution properties are shown in Table 6.

Table 6. Five test solutions used in the capillary suction tests with their associated dynamic viscosities and densities at 30 °C.

Glycerol (wt%)	Dynamic Viscosity (cP)	Density (g/mL)
0	0.8	0.996
15	1.2	1.027
25	1.6	1.053
30	1.9	1.069
35	2.2	1.081

2.3. Column Design and Packing Methodology

The experimental rig used for the bed characterisation and tracer tests is shown in Figure 3. The polyvinyl chloride column used in the tests had an inner diameter of 100 mm and a total height of 500 mm (Figure 4). A standard bed height of 160 mm was used for the tests (Figure 5). The column was irrigated from the top using a peristaltic pump (Cole

Palmer; MasterFlex L/S; Model no: 7528-10). A concentric drainage plate consisting of ± 3 mm apertures was placed approximately 60 mm from the base of the column to provide a liquid disengagement area. The heating coils wrapped externally around the column, a temperature probe inserted into the port immersing it 10 cm into the bed, together with the temperature control box were used to maintain the temperature within the column at 30 °C.

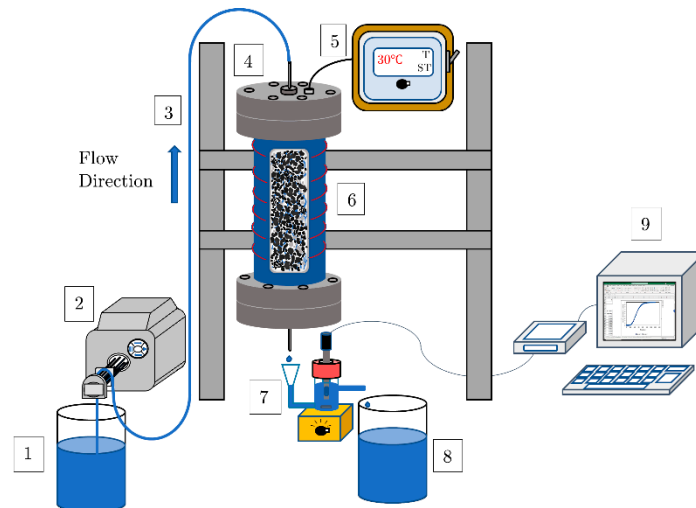


Figure 3. Illustration of the experimental set-up used to conduct tracer tests on the packing materials. It consisted of a (1) 20 L feed tank, (2) peristaltic pump, (3) tubing, (4) cylindrical test column, (5) temperature control unit, (6) heating coils, (7) conductivity measurement cell, (8) 20 L effluent tank, and (9) a desktop computer with data logging software (Graphical Analysis 4).

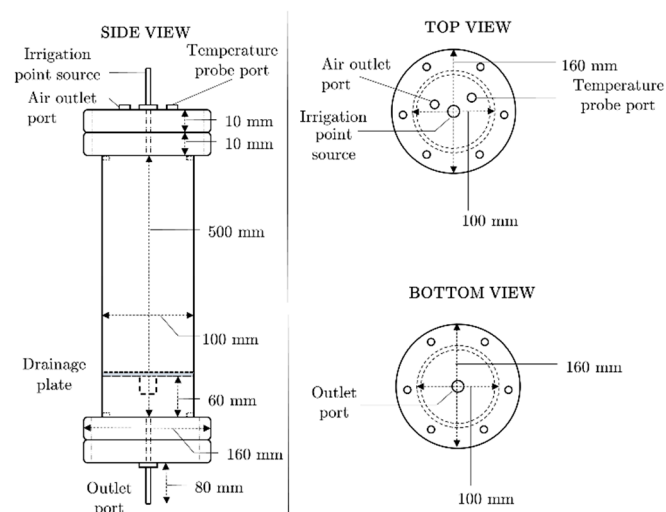


Figure 4. Cylindrical column design and dimensions used in tracer tests [29].

Agglomeration of the mixed size fractions was carried out by loading the specified mass of material into a plastic bucket. A measured volume of agglomeration solution, identical to the irrigation solution that would be used but without the tracer, was poured onto the surface of the material. The bucket was then rotated manually in a clockwise and anti-clockwise direction until the successful adhesion of fines to coarser particles was visually observed. No binders were used and this methodology is referred to as drum agglomeration [30]. The total amount of agglomeration moisture used was noted.

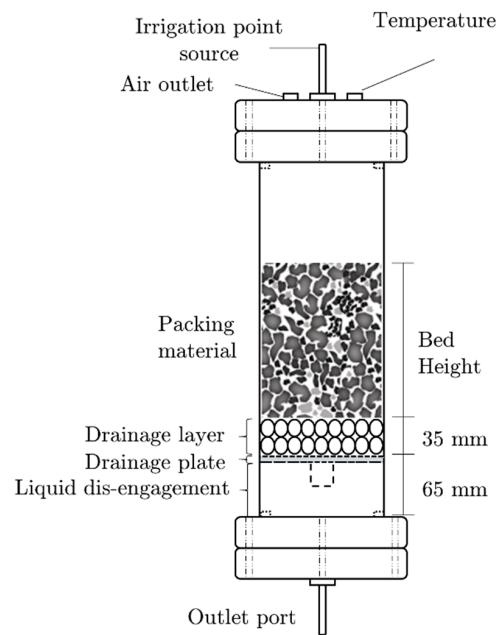


Figure 5. Illustration of the cylindrical column packing [29].

A drainage layer, approximately 35 mm in height, consisting of two layers of 24 mm glass marbles was inserted at the base of the column to prevent clogging and the elution of fines (Figure 5). The column was loaded by pouring small incremental masses of dry or agglomerated material onto the drainage layer using a scoop without any attempt of compaction.

For the mixed particle size beds, the Gates–Gaudin–Schumann distribution function, shown in Equation (1), was used to obtain the mass of material needed per size fraction. The cumulative fraction (R_F) of particles with a diameter less than or equal to d_p was calculated by raising the quotient of the selected and maximum particle diameter ($d_{p,max}$) to the power of m . The Gates–Gaudin–Schumann distribution has been used by other studies as a means of characterising the size distributions of different particle aggregates, especially those related to leach beds [7,31,32]. For this study, m was chosen to equal 0.4 in order to mimic industrial ores typical of heap leaching and the resulting size distribution for the various mixtures is presented in Figure 6. The top particle size was kept constant at 8 mm whilst the bottom particle size was systematically increased from 0.1 to 0.5 to 1 mm, simulating the exclusion of fines.

$$R_F(d_p) = \left(\frac{d_p}{d_{p,max}} \right)^m \tag{1}$$

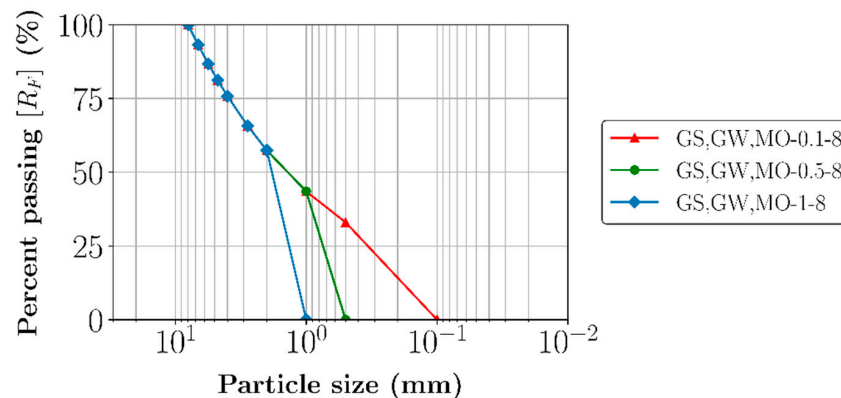


Figure 6. Particle size distributions for the packed beds composed of the different sized mixtures.

2.4. Packed Bed Characterisation

The packed bed systems were characterised using five main experimental parameters: bulk density, bed voidage, solution breakthrough time, liquid hold-up, and 24-h drain-down moisture.

The bulk densities were calculated by dividing the total mass of the dry bed's contents by its volume. Liquid-accessible bed voidage was defined as the ratio of the void volume (empty space) present within the bed to its total volume. It was obtained at the end of each tracer test by gradually filling the bed's void spaces with irrigation solution pumped upwards at a rate of 9 mL/min.

Solution breakthrough time was defined as the time difference between irrigation commencement and the emergence of the first fluid droplets at the bottom of a packed bed. Similarly, the steady-state tracer breakthrough time was defined as the time difference between the commencement of the tracer test and the time at which the first distinct rise in tracer concentration in the bed's effluent was measured. Liquid hold-up (ϕ_l) was defined as the ratio of liquid volume (V_l) to total bed volume (V_b) in an irrigated packed bed at steady-state, as shown by Equation (2). The 24-h drain-down moisture values were obtained at the end of each tracer test by measuring the volume of solution collected in a 24-h period after irrigation was stopped. It is expressed as a percentage of total liquid hold-up.

$$\phi_l = \frac{V_l}{V_b} \quad (2)$$

2.5. Irrigation and RTD Testing of Packed Columns

The packed columns were irrigated at an average flux of 5 L/(m²·h) from the singular irrigation point source shown in Figures 4 and 5. The step input form of tracer delivery was used for all tracer tests. Potassium chloride (KCl) was selected as a salt tracer due to prior tests confirming that it had negligible effect on a solution's viscosity and density within the applied range and was non-adsorbent. At the start of the tests, a 0.01 mol/L KCl feed solution was used to irrigate the beds at the average flux. This was carried out until a steady-state was achieved, defined as when the volumetric flow rate of solution fed into the bed equaled the flow rate out of the bed. The feed was then changed to a tracer solution with a maximum concentration of 0.1 mol/L KCl solution. The conductivity of the column's effluent was monitored continuously using a conductivity measurement cell, which consisted of a cylindrical glass vessel housing a Vernier conductivity probe. Mixing effects within the conductivity measurement cell were accounted for using a back-modelling approach, which assumed the solution to be perfectly mixed within the cell [33]. The resulting data were normalised to produce the cumulative RTD curves.

2.6. RTD Analysis

The logged conductivity data, which represented the cumulative residence time distribution or F-curve, were normalised with respect to the maximum tracer concentration, as shown by Equation (3). The residence time distribution or E-curve was then derived from the derivative of the F-curve using Equation (4). For graphical representation, the generated E-curves were smoothed using a five-point moving average numerical technique.

$$F(t) = \frac{C(t)}{C_0} \quad (3)$$

$$E(t) = \frac{dF(t)}{dt} = \frac{d}{dt} \left[\frac{C(t)}{C_0} \right] \quad (4)$$

Three different RTD parameters or moments were quantified from the derived E-curves: the average residence time, the standard deviation, and the skewness. The average residence time (τ , first moment) was calculated using Equation (5). The standard deviation, which is the square-root of the variance (σ , second moment), was calculated using Equation (6) and the skewness (δ , third moment) was calculated using Equation (7).

$$\tau = \int_0^{\infty} tE(t) dt \quad (5)$$

$$\sigma = \sqrt{\int_0^{\infty} (t - \tau)^2 E(t) dt} \quad (6)$$

$$\delta = \frac{1}{\sigma^{3/2}} \int_0^{\infty} (t - \tau)^3 E(t) dt \quad (7)$$

The equations were coded using the Python programming language and the Scientific Python Development Environment (Spyder) version 4.1.5.

2.7. Diagnosing Preferential Flow Characteristics

Referential flow characteristics in irrigated beds were diagnosed using the RTD profiles and bed characterisation parameters. Low levels of total liquid hold-up with quick solution and tracer breakthrough times are typical symptoms of bed-scale preferential flow or channelling. These are prime indications of non-uniform wetting and hence, maldistribution of irrigated solution within the bed. Solution-scale preferential flow characteristics are normally diagnosed through the analysis of the steady-state RTD profiles. In this case, profiles with long asymptotes indicate the presence of stagnant or slow-moving solution volumes. The level of skewness in the dataset and the standard deviation values help to quantify the length of the asymptote and hence, the degree of solution-scale preferential flow. In cases where the RTD responses for systems with similar liquid hold-ups are substantially different, isolated fluid volumes are likely present in the system with the shorter tracer breakthrough times. These volumes form during the wetting stage of the bed but become isolated from all forms of fluid and solute transport at steady-state fluid flux. Therefore, the steady-state RTD profile would not reflect the presence of these volumes.

3. Results and Discussion

3.1. Effect of Particle Shape

The RTD profiles and bed characterisation results for the spherical GB and irregularly shaped GS can be found in Figures 7 and 8, respectively. Table 7 gives a summary table of the various parameters. Both these systems were non-porous with similar compositions, meaning that particle shape was their main differentiating factor.

Differences in the RTD profiles of the systems are more noticeable at the 1–3 mm size range (Figure 7a,b). The GB-2 bed showed slightly greater levels of solution channelling behaviour compared to the GS-1-2 and GS-2-3 systems. This is reflected in the 7 to 19 min shorter solution breakthrough time (refer to Figure 8d) as well as the approximately 55% shorter average solute residence time (τ) value obtained for the GB-2 bed (refer to Table 7). From these results, increased particle sphericity at the 1–3 mm range resulted in increased channelling effects both during the initial wetting stages of the beds (solution breakthrough time) and after the establishment of steady-state fluid flux (RTD profiles).

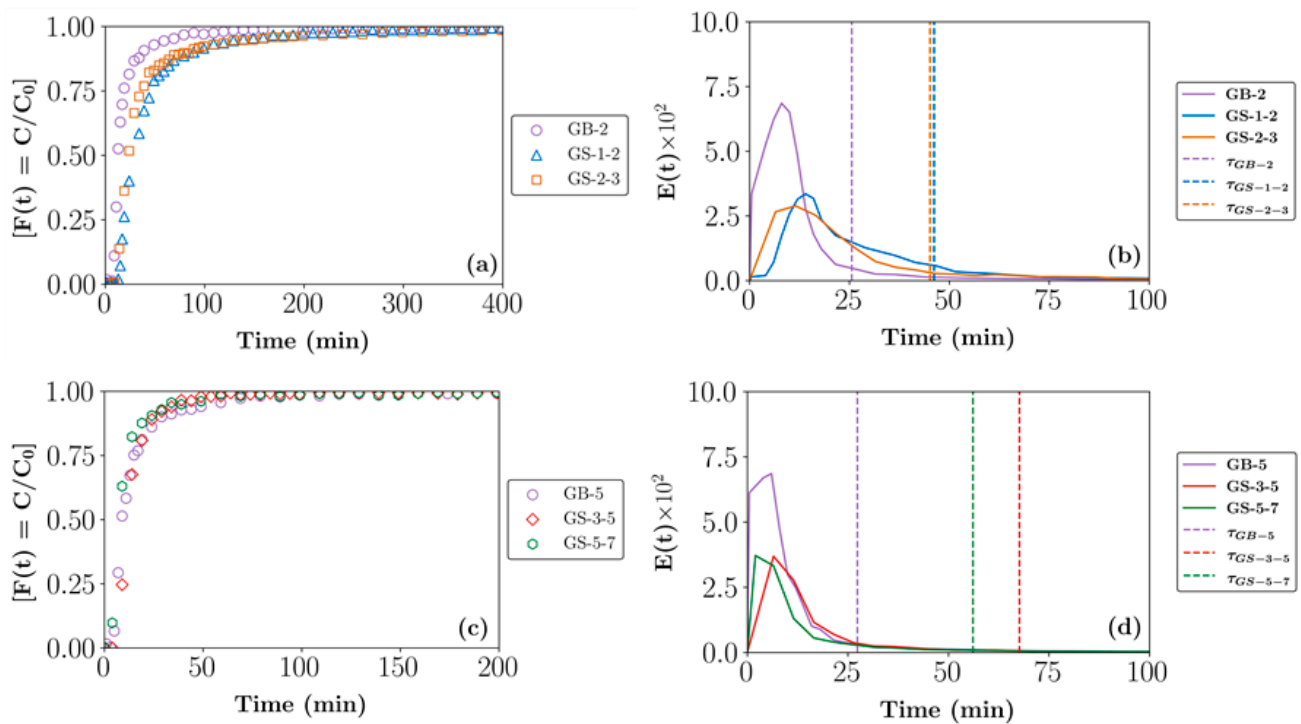


Figure 7. (Left—(a,c)) Cumulative $F(t)$ and (right—(b,d)) exit age $E(t)$ RTD profiles for beds composed of different size fractions of glass beads (GBs) and glass shards (GSs). Key: GB-2 (2 mm), GB-5 (5 mm), GS-1-2 (1–2 mm), GS-2-3 (2–2.8 mm), GS-3-5 (2.8–4.8 mm), and GS-5-7 (4.8–6.7 mm).

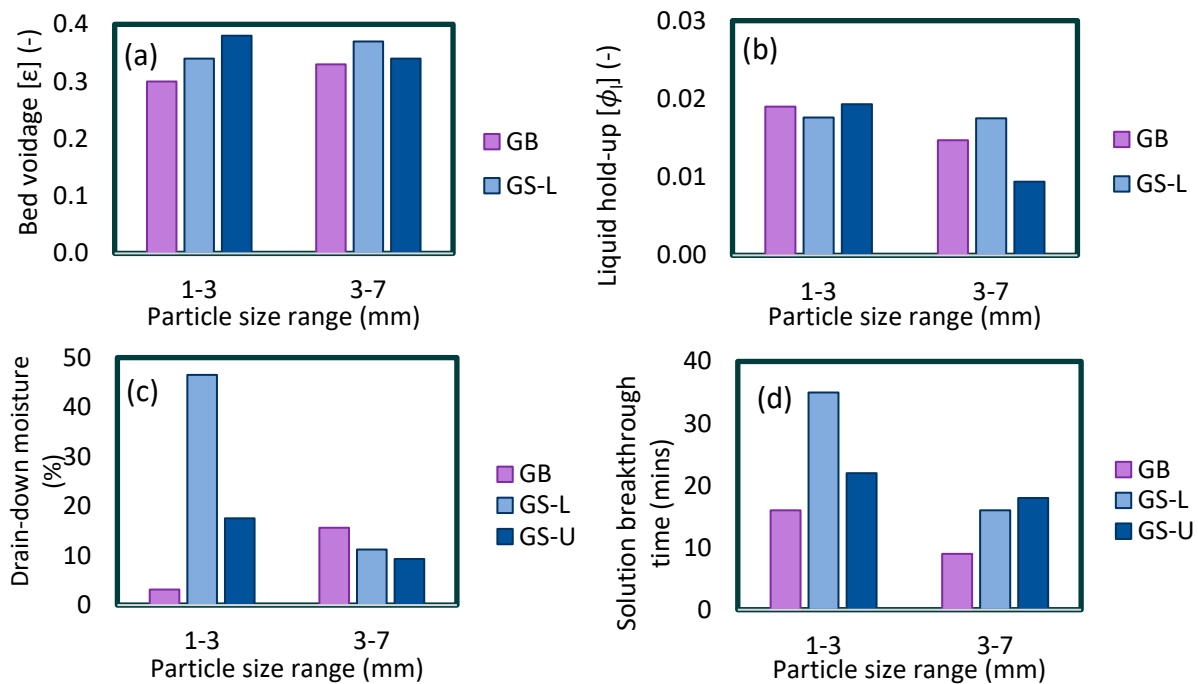


Figure 8. (a) Bed voidage, (b) total liquid hold-up, (c) 24-h drain-down moisture as the percentage of total liquid hold-up and (d) solution breakthrough time characterisation data for beds composed of different size fractions of GBs and GSs. Key: L—lower size range; U—upper size range; GB 1-3 size range (GB-2) and GB 3-7 size range (GB-5); GS-L 1-3 size range (GS-1-2) and GS-L 3-7 size range (GS-3-5); GS-U 1-3 size range (GS-2-3) and GS-U 3-7 size range (GS-5-7).

Table 7. Bed characterisation and quantified RTD parameters for packed beds composed of different size fractions of GSs, GW, and MO. Key: E-tag (experimental tag), PSD (particle size distribution), BD (bulk density), BV (bed voidage), LH (total liquid hold-up), DM (24-h drain-down moisture as a percentage of total liquid hold-up), and BT (solution breakthrough time).

Packing	E-Tag	PSD (mm)	Bed Characterisation Parameters				RTD Parameters			
			BD (g/cm ³)	BV (-)	LH (-)	DM (%)	BT (mins)	τ (mins)	σ	δ
Glass beads	GB-2	2	1.58	0.30	0.02	3.1	16	26	35	3.51
	GB-5	5	1.45	0.33	0.01	15.6	9	18	22	3.01
Glass shards	GS-1-2	1.0–2.0	1.22	0.34	0.02	46.5	35	46	47	2.65
	GS-2-3	2.0–2.8	1.15	0.38	0.02	17.5	22	45	67	4.19
	GS-3-5	2.8–4.8	1.33	0.37	0.02	11.2	16	17	12	2.26
	GS-5-7	4.8–6.7	1.32	0.34	0.01	9.3	18	14	16	2.81
	GS-7-8	6.7–8.0	1.29	0.38	0.02	2.8	8	15	15	1.93
	GS-0.1-8	0.1–8.0	1.20	0.31	0.14	12.5	210	291	174	1.88
	GS-0.5-8	0.5–8.0	1.13	0.33	0.08	47.0	95	167	121	2.31
	GS-1-8	1.0–8.0	1.22	0.43	0.06	32.5	53	105	150	3.30
Greywacke	GW-1-2	1.0–2.0	1.25	0.33	0.05	87.5	68	186	240	1.99
	GW-2-3	2.0–2.8	1.25	0.40	0.09	50.2	67	158	234	2.39
	GW-3-5	2.8–4.8	1.24	0.39	0.08	38.2	35	86	119	2.80
	GW-5-7	4.8–6.7	1.22	0.40	0.05	34.0	36	172	279	1.39
	GW-7-8	6.7–8.0	1.26	0.42	0.06	32.8	23	94	162	2.47
	GW-0.1-8	0.1–8.0	1.22	0.32	0.14	17.2	198	316	271	1.75
	GW-0.5-8	0.5–8.0	1.13	0.35	0.09	49.3	77	197	178	2.23
	GW-1-8	1.0–8.0	1.23	0.44	0.08	38.6	39	132	204	2.34
Malachite ore	MO-1-2	1.0–2.0	1.02	0.48	0.15	25.9	255	290	183	1.28
	MO-2-3	2.0–2.8	1.00	0.49	0.15	31.6	75	236	207	1.78
	MO-3-5	2.8–4.8	1.07	0.43	0.11	30.4	51	143	229	2.32
	MO-5-7	4.8–6.7	1.00	0.45	0.10	29.3	46	190	234	1.08
	MO-7-8	6.7–8.0	1.01	0.49	0.09	19.0	21	100	161	2.17
	MO-0-8	0.0–8.0	1.19	0.44	0.26	10.4	302	548	272	0.78
	MO-0-8 (1.2cP)	0.0–8.0	1.20	0.44	0.24	13.4	296	485	230	-0.35
	MO-0-8 (1.6cP)	0.0–8.0	1.17	0.47	0.27	15.4	334	499	217	-0.35
	MO-0-8 (1.9cP)	0.0–8.0	1.18	0.51	0.32	11.9	255	514	226	-0.31
	MO-0-8 (2.2cP)	0.0–8.0	1.19	0.46	0.23	16.9	245	470	236	-0.03
	MO-0.1-8	0.1–8.0	1.21	0.41	0.17	16.9	229	396	272	1.11
MO-0.5-8	0.5–8.0	1.10	0.45	0.15	28.4	174	317	147	1.17	
MO-1-8	1.0–8.0	1.19	0.51	0.13	36.8	168	287	202	1.12	

The GS systems had higher standard deviation values (refer to Table 7) which reflect the greater spread in their E-curves. This is indicative of the presence of fluid elements with relatively long residence times. It is likely that the flatter and longer shape of the shards

resulted in a higher number of particle contact points, which increased the probability of the redirection of flow away from the central irrigation axis. This is based on results from Fernando et al. [9] and the understanding that lateral spread leads to greater variation in fluid residence times in single point drip-irrigated systems. All three systems in the 1–3 mm size range attained similar total liquid hold-up values (refer to Figure 8b), which were relatively low and averaged around 0.02, yet the GB-2 RTD profiles still displayed slightly enhanced channelling effects, which points towards the presence of isolated solution volumes within the bed. Based on Ilankoon and Neethling [11], the liquid rivulets flowing across the irregularly shaped shards are likely to have greater tortuosity which could result in increased connectivity compared to the beads. This is supported by the 24-h drain-down moisture data, which were significantly lower for the GB-2 system (3.1%) than for the shards (17%–47%). Additionally, the spherical nature of the 2 mm beads resulted in a denser packing arrangement (refer to Figure 8a), typical of the trend found in the literature [9], therefore the similar liquid hold-up values at the 1–3 mm size range also meant that the absolute mass of fluid retained in the GB-2 bed was lower.

3.2. Effect of Wettability and Porosity

The RTD profiles and bed characterisation data for the GS, GW, and MO mixed sized beds are shown in Figures 9 and 10. Table 5 gives a summary of the main features of the different packing materials. Regarding particle wettability, the highly hydrophilic GW beds had the quickest tracer and solution breakthrough times across all three sets of systems (refer to Figures 9a,c,e and 10d). Therefore, increased particle wettability led to slightly higher dispersive effects, during both the initial wetting period and at steady-state. The irrigation fluid experienced less resistance to flow across the GW particles' surfaces, which enhanced channelling through the bed. However, the similarities between the GS and GW system and their substantial differences between the highly porous MO beds, points towards particle porosity being the main differentiating factor in the responses of the systems.

In terms of porosity, the non-porous GS beds obtained the lowest solute residence times compared to the porous GW and MO systems whose RTD profiles exhibited slightly longer asymptotes. The average voidage of heaps is thought to be around 0.4 [7,34], meaning that only the MO beds were able to achieve and exceed this value with the random, non-compacted packing method employed. These highly porous beds had the longest average residence times, longest tracer breakthrough times, and consistently higher liquid hold-up and higher drain-down moisture percentages (refer to Figure 10b,c). The fact that the MO systems had the lowest magnitudes of skewness in their E-curves and the lowest peaks (refer to Figure 9b,d,f and Table 7) points towards greater uniformity in the spread of the data. Therefore, these systems exhibited the widest distribution of fluid residence times, which is indicative of a larger number of fluid flow paths. It is postulated that the MO beds possessed higher degrees of void network connectivity and capillary suction, which allowed for greater lateral spread of irrigated solution evidenced by higher levels of liquid hold-up. The longer asymptotes in the MO systems should be noted as they point towards the increased presence of stagnant solution pools. This suggests that though material porosity promotes uniform wetting via capillary action, the solution pools formed may not remain actively flowing during steady-state. A similar point was raised by Ilankoon and Neethling [8,35].

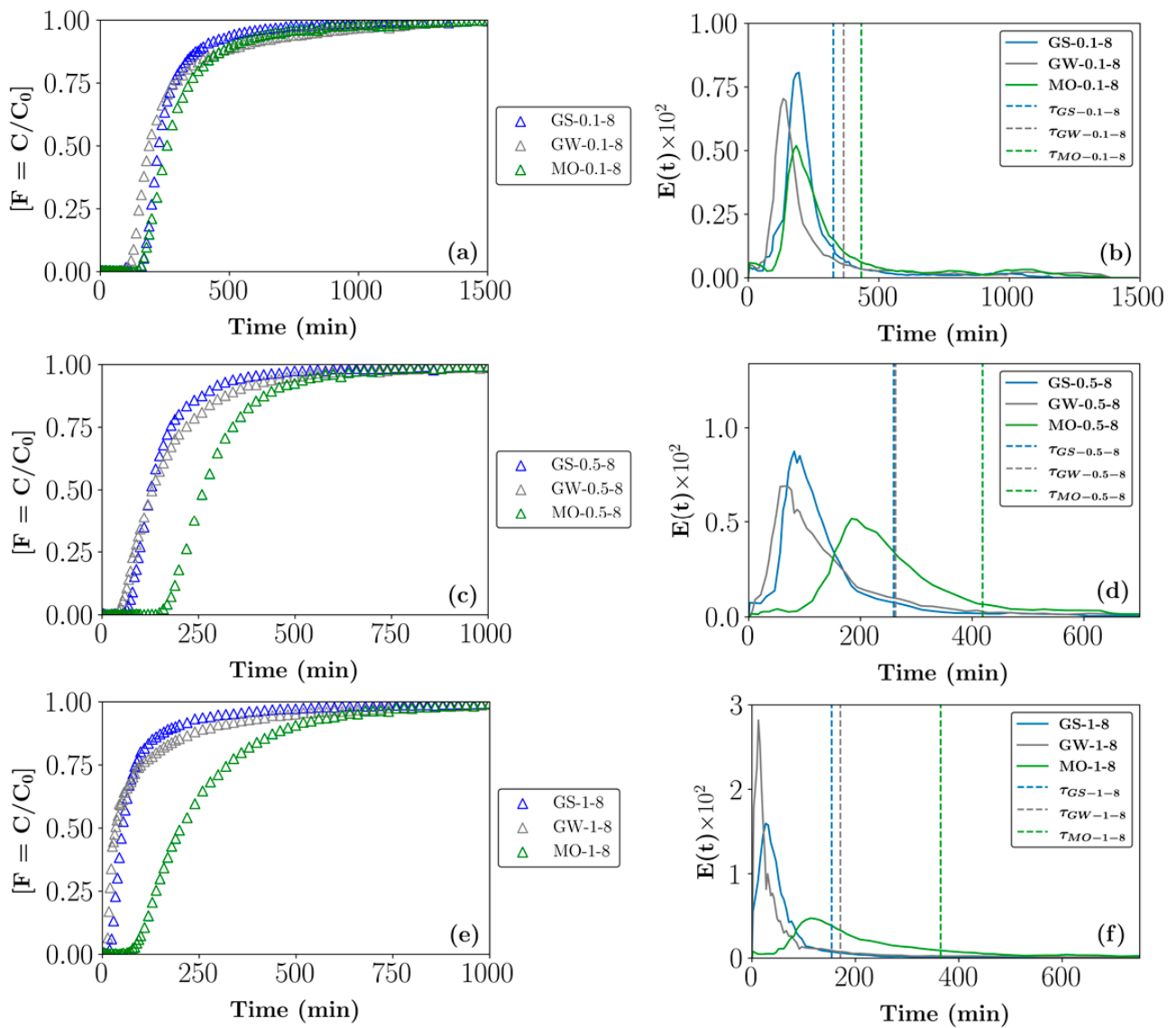


Figure 9. (Left—(a,c,e)) Cumulative ($F(t)$) and (right—(b,d,f)) exit age ($E(t)$) RTD profiles for beds composed of different size fractions of GSs, GW, and MO. The vertical lines in the $E(t)$ curves represent the calculated average residence times. Key: GS/GW/MO- 0.1-8 (0.1–8 mm), 0.5-8 (0.5–8 mm), and 1-8 (1–8 mm).

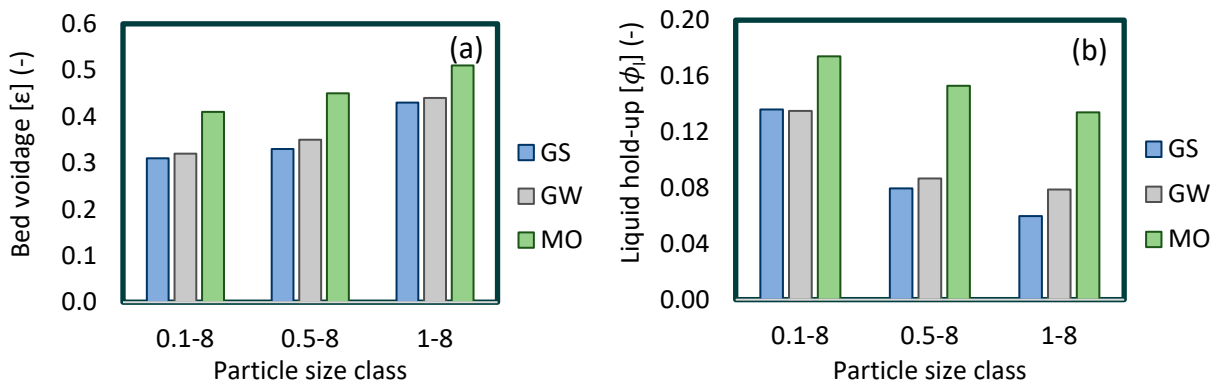


Figure 10. Cont.

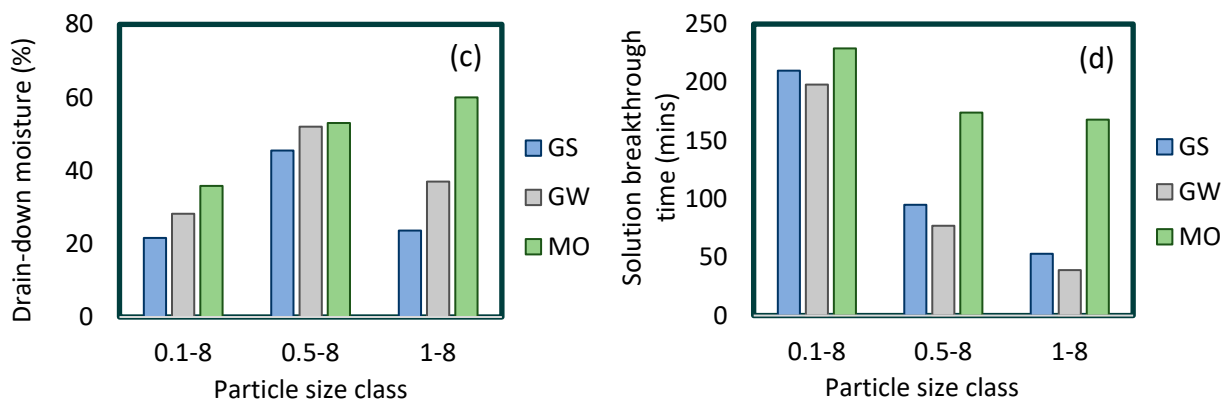


Figure 10. (a) Bed voidage, (b) total liquid hold-up, (c) 24-h drain-down moisture as percentage of total liquid hold-up, and (d) solution breakthrough time characterisation data for beds composed of different size fractions of GSs, GW, and MO. Key: 0.1-8 (0.1–8 mm), 0.5-8 (0.5–8 mm), and 1-8 (1–8 mm).

3.3. Effect of the Systematic Exclusion of Fines

Figures 9 and 10 show the effect of systematically excluding fines from the particle size distribution of mixed sized beds. Increasing the bottom size limit of the non-porous GS and moderately porous GW beds from 0.1 to 1 mm brought about significant reductions in their total liquid hold-up (43%–57%), solution (75%–80%), and tracer (80%–90%) breakthrough times. Though the liquid hold-up for the 0.5–8 mm and 1–8 mm systems (excluding the MO beds) are similar, differences in their (GS and GW) steady-state RTD curves (Figure 9c,e) are noticeable. This suggests an increase in the formation of isolated fluid volumes with the decrease in the presence of agglomerated fines for the less porous beds. The MO systems' RTD responses were more resistant to changes in bottom particle size. In fact, the RTD profiles for the MO-0.1-8 and MO-0.5-8 beds are nearly identical. It is only when the bottom size was further raised to 1 mm that a reduction in the tracer breakthrough time was observed. Furthermore, the MO system experienced the lowest reduction in total liquid hold-up (29%) and solution breakthrough time (27%) with the increase in bottom particle size.

Based on these results, the exclusion of fines from the particle size distribution of mixed sized beds can be extrapolated to have reduced the strength of capillary forces present within the beds, as reported by Yin et al. [36] and Odidi et al. [37]. As these are suctioning forces that facilitate the absorbance of moisture during the wetting stage, a decrease in their strength results in a reduction in liquid hold-up, tracer, and solution breakthrough time as well as an increase in isolated fluid volumes. Higher levels of particle porosity act as a buffer against these responses, allowing the beds to maintain their liquid hold-up values and RTD profile characteristics even when fines are excluded to a certain extent. What is therefore important in these systems are the size distributions and connectivity of the void network through which the irrigated solution travels, meaning that both an increase in porosity and the inclusion of fines in agglomerates produce similar effects. One such effect is an increase in the fraction of stagnant solution volumes.

3.4. Culminative Effect of Narrow Size Fractions in Mixed Sized Beds

The bed characterisation and RTD profile results for the beds composed of narrow and mixed size fractions ranging from 1 to 8 mm are shown in Figures 11 and 12.

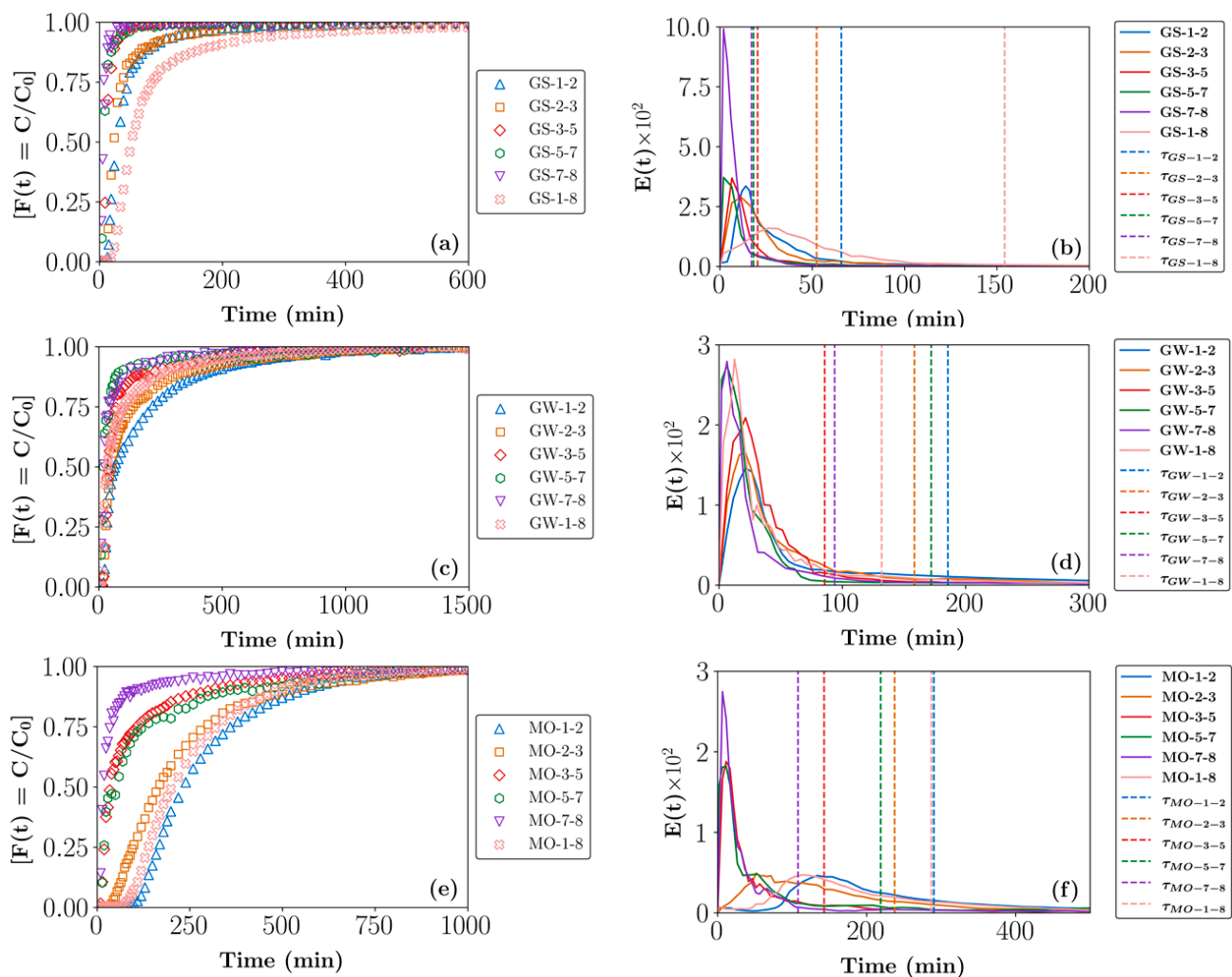


Figure 11. (Left—(a,c,e)) Cumulative ($F(t)$) and (right—(b,d,f)) exit age ($E(t)$) RTD profiles for beds composed of different size fractions of glass shards (GSs), greywacke (GW), and malachite ore (MO). The vertical lines in the $E(t)$ curves represent the calculated average residence times. Key: GS/GW/MO- 1-2 (1–2 mm), 2-3 (2–2.8 mm), 3-5 (2.8–4.8 mm), 5-7 (4.8–6.7 mm), 7-8 (6.7–8 mm), and 1-8 (1–8 mm).

For the non-porous GS systems (Figure 11a,b), increasing the narrow size fraction from 1–2 mm to 6.7–8 mm brought about an increase in solution channelling behaviour both prior to and during steady-state fluid flux. This is based on the 77% reduction in solution breakthrough time from 35 to 8 min as well as the 6-min reduction in tracer breakthrough time. The RTD profiles for the GS-3-5 to GS-7-8 systems all attained maximum tracer concentrations ($F = 0.99$) within 2 h of the commencement of the tracer tests compared to the GS-1-2 and GS-2-3 beds which only attained this value after 5 to 8 h. This is also seen in the approximately 67% reduction in the average residence time values when comparing the smaller particle size systems to the larger ones. It is interesting to note that the results for the mixed system (GS-1-8) are unique and not an average of its narrow size constituents. The GS-1-8 bed exhibited the longest solution and tracer breakthrough times, the highest liquid hold-up, and the longest average steady-state residence time.

From these results, increasing the material gradation of the non-porous GS beds reduced bed-scale preferential flow symptoms based on its higher liquid hold-up. The prime mechanism for this increase in wetting behaviour was likely the increase in particle connections leading to enhanced lateral spread of irrigated solution as reported by Ilankoon and Neethling [8]. In cases where only large particles were present, macro-voids were

likely formed between the particles allowing for the channelling of irrigated solution by gravitational forces along the central–vertical irrigation axis. When small particles were present to fill the gaps between large particles, meso- and micro-voids would be present in greater numbers enhancing the lateral spread of solution by capillary forces. In addition, the larger length scale of the non-porous uniquely shaped agglomerates in the mixed size bed is postulated to have led to increased mechanical dispersion based on results by Fernando et al. [9], which allowed it to acquire greater liquid hold-up compared to the GS-1-2 bed.

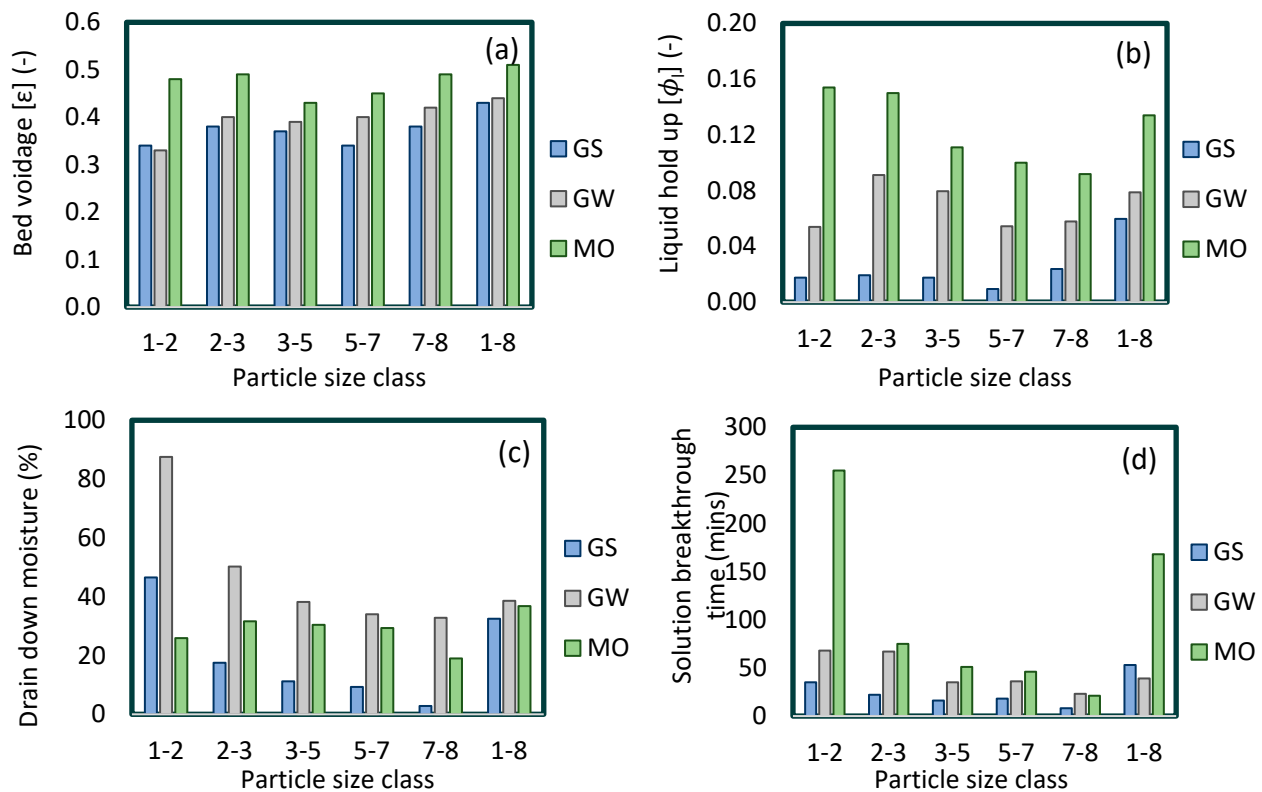


Figure 12. (a) Bed voidage, (b) total liquid hold-up, (c) 24-h drain-down moisture, and (d) solution breakthrough time characterisation data for beds composed of different size fractions of GS, GW, and MO.

The beds composed of the hydrophilic and moderately porous GW particles exhibit a similar trend to the GS beds in terms of an increase in channelling behaviour with an increase in narrow size fraction. Unlike the shards, however, the channelling behaviour at steady-state with the increase in size fraction, from 1–2 mm to 6.7–8 mm, does not involve any substantial decrease in tracer breakthrough time. There was instead an approximate 3-h decrease in the time required for the GS-7-8 bed to attain the maximum level of tracer concentration. There are two reasons for this. Firstly, all the GW beds possessed relatively short tracer breakthrough times regardless of particle size distribution due to the hydrophilic nature of the particles. Secondly, the presence of larger particles brought about a reduction in the average fluid residence times likely due to the formation of larger size voids and a reduction in capillary effects. The RTD response for the mixed size bed (GW-1-8) appears to be an average of the responses of its narrow size fraction constituents. It is possible that a majority of the agglomerates formed were similar in size to the GW-1-3 and GW-3-5 beds, hence the comparable results. Unlike the non-porous GS, the GW beds were less reliant on mechanical dispersion for lateral spread of irrigated solution and more influenced by wettability and capillary effects, hence the difference in their responses to changes in particle size distributions.

The highly porous MO beds all possessed effective voidage values greater than 0.4 and followed the same trend as the other systems with a 50% and 92% reduction in tracer and solution breakthrough time, respectively, with an increase in size fraction from 1–2 mm to 6.7–8 mm. A substantial change in the RTD responses can be observed between the 2–2.8 mm and 2.8–4.8 mm size ranges as channelling effects became more dominant with further increases in size fraction. It is interesting that most of the bed characterisation parameters and RTD responses for the mixed bed (MO-1-8) were very similar to those of the MO-1-2 system. This suggests that the incorporation of particles in the 1 to 2 mm size range, and hence enhanced capillary effects, was the dominant factor influencing the flow characteristics of the mixed size bed. However, the presence of the larger particles in the MO-1-8 system had a comparably smaller effect on its RTD profile compared to the GW beds. This is likely due to the highly porous nature of the MO particles, which still managed to maintain sufficient levels of capillary effects even at larger particles sizes and facilitated the lateral spread of irrigated solution evidenced by the relatively high liquid hold-up in the mixed size bed.

3.5. Effect of Solution Viscosity in Mixed Size Beds

The results of the effect of solution viscosity on the RTD profiles and bed characterisation parameters of mixed size malachite ore beds can be found in Figures 13 and 14. The range of viscosity values used (0.8 to 2.2 cP) is representative of an increase in the ionic concentration of typical sulphate leach solutions (0 to >100 g/L SO_4^{2-}).

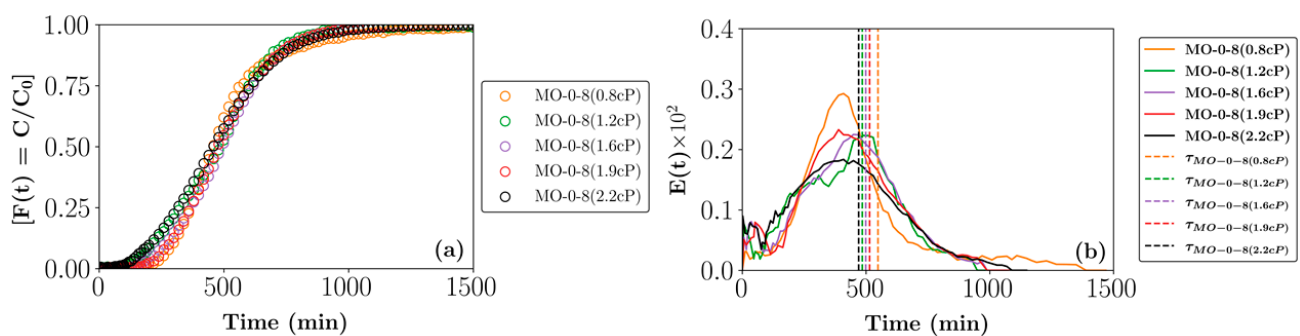


Figure 13. (Left—(a)) Cumulative ($F(t)$) and (right—(b)) exit age ($E(t)$) RTD profiles for beds composed of 0–8 mm MO particles and irrigated with different viscosity solutions (0.8, 1.2, 1.6, 1.9, and 2.2 cP). The vertical lines in the $E(t)$ curves represent the calculated average residence times.

Increasing the irrigation fluid's viscosity from 0.8 to 2.2 cP brought about a 19% decrease in the solution breakthrough time from 302 to 245 min and a 50% reduction in tracer breakthrough time from 199 to 99 min. There is evidence of an increase in dispersive effects as well, especially during the initial parts of the F -curves (refer to Figure 13a). However, there was a 22% reduction in the time taken for the more viscous system (2.2 cP) to achieve the maximum tracer concentration, which indicates an overall shift in the RTD profiles to the left. This observation is consistent with the decrease in the average residence times. It is interesting to note the slightly negative skewness values obtained for the 1.2 to 2.2 cP systems which shows that the E -curves for these systems were nearly symmetrical but marginally skewed to the right showing a decrease in the length of the asymptotes or stagnant volumes. No consistent trends with regards to the effect of viscosity on total liquid hold-up were observed but an overall positive correlation with the percentage of drain-down moisture is seen in Figure 14c.

From these results, it is postulated that though an increase in the viscosity increases a solution's resistance to flow, this effect is counteracted by the increase in the solution's density, making it more susceptible to gravitational forces and thereby leading to greater levels of axial spread or dispersion at steady-state. At first glance, the increase in drain-down moisture percentage suggests that a higher proportion of the liquid hold-up volumes

in the higher viscosity systems were active, which correlates with the decrease in the length of the asymptotes in the RTD profiles. However, all the systems still had droplets emerging from the column after the 24-h drain-down period. It could also be that the more viscous systems possessed higher drainage velocities allowing for a greater volume of solution to be collected within the allocated time, based on a drainage behaviour study by Ilankoon and Neethling [11]. Again, effects due to differences in fluid densities would be at play. There is also slight evidence of the increased presence of isolated fluid volumes in the more viscous systems at steady-state based on their RTD profiles and liquid hold-up data. This suggests that once the wetting stage was complete, there was channelling of fluid down the central irrigation axis with reduced lateral exchange of material at steady-state.

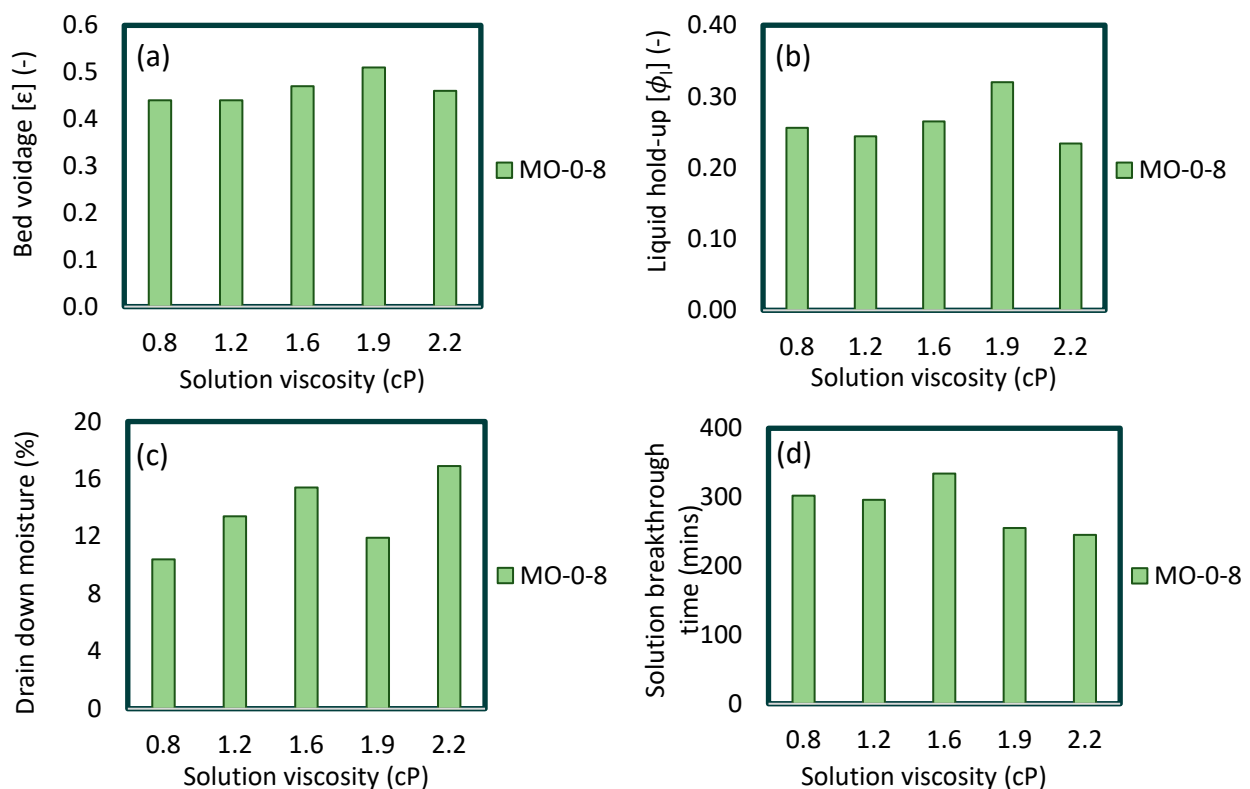


Figure 14. (a) Bed voidage, (b) total liquid hold-up, (c) 24-h drain-down moisture, (d) solution breakthrough time characterisation data for beds composed of 0–8 mm MO particles and irrigated with different viscosity solutions (0.8, 1.2, 1.6, 1.9, and 2.2 cP).

4. Conclusions

This study aimed to quantify the effect that particle shape, porosity, wettability, size fraction, size distribution, and irrigation solution viscosity have on the bed characterisation parameters and RTD profiles of different ore bed systems representative of heap leaching. Step-up salt tracer tests were used to obtain the RTD profiles which were then analysed to quantify different RTD parameters.

Of the inherent properties of the materials tested, particle porosity exerted the most influence on the flow profiles and bed characterisation parameters obtained. The results indicate that drip-irrigated highly porous heaps are more likely to be evenly wetted due to enhanced capillary effects. However, even with enhanced wetting, active solution flow may still be restricted in highly porous heaps due to strong capillary forces. A balance is needed to ensure wetting but to reduce stagnant solution volumes. The data obtained suggest that imposing limits on the fine content (e.g., >0.1 mm bottom size) or increasing the proportion of larger size particles (e.g., >7 mm) could aid in reducing the fraction of these volumes.

The results from the mixed size beds emphasise the importance of the inclusion of fines (<1 mm) in agglomerates to aid in the lateral spreading of drip-irrigated solution by capillary action. This is more necessary in cases where the ore particles have low to moderate inherent levels of porosity (<2 m²/g). However, the positive correlation between high fine contents and the relative magnitude of stagnant solution volumes should be borne in mind.

Though the results indicate that increasing the irrigation solution viscosity from 0.8–2.2 cP (representative of an increase in sulphate ionic concentration from 0 to >100 g/L SO₄²⁻ in reactive heaps) may not affect the overall wetting of a heap, it brings about greater levels of solution-scale preferential flow. It may also reduce the propensity for lateral movement in already wetted heaps. The level to which this occurred at the lab scale was not very significant, but an increase in scale will further elucidate if monitoring and management of viscosity in actual heap leaching operations is necessary.

It should be noted that the results from this study may not be applicable to ores with high clay and silica content as these compounds can lead to structural changes in irrigated beds with the potential to substantially affect fluid flow profiles.

Author Contributions: M.D.O.: conceptualisation, methodology, validation, formal analysis, investigation, data interpretation, writing—original draft, writing—review and editing, and visualisation; M.A.F.-E.: conceptualisation, methodology, resources, data interpretation, writing—review and editing, supervision, and project administration; S.T.L.H.: conceptualisation, methodology, resources, data interpretation, writing—review and editing, supervision, project administration, and funding acquisition. All authors have read and agreed to the published version of the manuscript.

Funding: This work is based on research supported through Mintek, South Africa, and by the National Research Foundation of South Africa through the South African Research Chairs Initiative (SARChI) Chair in Bioprocess Engineering (UID 64778). Any opinions, findings, conclusions or recommendations expressed in this material are those of the authors and the SARChI and NRF do not accept any liability in this regard.

Data Availability Statement: Figures, Microsoft Excel™ workbook and python code template used in this article are available at the following DOIs respectively: 10.25375/uct.21656375, 10.25375/uct.21666995 and 10.25375/uct.21667169.

Acknowledgments: Authors will like to thank the Centre for Minerals Research (CMR) at the University of Cape Town, for their help with sample preparation and analysis.

Conflicts of Interest: The authors declare no conflict of interest.

References

1. Satterfield, C.N. Trickle-Bed Reactors. *AIChE J.* **1975**, *21*, 209–228. [[CrossRef](#)]
2. Ghorbani, Y.; Franzidis, J.-P.; Petersen, J. Heap Leaching Technology—Current State, Innovations and Future Directions: A Review. *Miner. Process. Extr. Metall. Rev.* **2015**, *37*, 73–119. [[CrossRef](#)]
3. van Staden, P.J.; Robertson, S.W.; Gericke, M.; Neale, J.W.; Seyedbagheri, A. Maximising the Value Derived from Laboratory Testwork towards Heap Leaching Design. In Proceedings of the Fifth Southern African Base Metals Conference 2009, Kasane, Botswana, 27–31 July 2009. [[CrossRef](#)]
4. Govender-Opitz, E.; Kotsiopoulos, A.; Fagan-Endres, M.; Harrison, S.T.L. Insight into Solute and Microbial Transport in Heap (Bio)Leaching Systems Using Residence Time Distribution. *Hydrometallurgy* **2017**, *168*, 1–6. [[CrossRef](#)]
5. Trincherio, P.; Beckie, R.; Sanchez-Vila, X.; Nichol, C. Assessing Preferential Flow through an Unsaturated Waste Rock Pile Using Spectral Analysis: Preferential Flow through a Waste Rock Pile. *Water Resour. Res.* **2011**, *47*, W07532. [[CrossRef](#)]
6. Wu, A.; Yin, S.; Yang, B.; Wang, J.; Qiu, G. Study on Preferential Flow in Dump Leaching of Low-Grade Ores. *Hydrometallurgy* **2007**, *87*, 124–132. [[CrossRef](#)]
7. Bouffard, S.C.; Dixon, D.G. Investigative Study into the Hydrodynamics of Heap Leaching Processes. *Met. Mater. Trans B* **2001**, *32*, 763–776. [[CrossRef](#)]
8. Ilankoon, I.M.S.K.; Neethling, S.J. Inter-Particle Liquid Spread Pertaining to Heap Leaching Using UV Fluorescence Based Image Analysis. *Hydrometallurgy* **2019**, *183*, 175–185. [[CrossRef](#)]
9. Fernando, W.A.M.; Ilankoon, I.M.S.K.; Rabbani, A.; Chong, M.N. Applicability of Pore Networks to Evaluate the Inter-Particle Flow in Heap Leaching. *Hydrometallurgy* **2020**, *197*, 105451. [[CrossRef](#)]

10. Fernando, W.A.M.; Ilankoon, I.M.S.K.; Krishnan, S.G.; Chokshi, V. The Effects of Packing Shape and Structure on Liquid Distribution of Heap Leaching Systems: Addition of PCBs as Non-Ore Particles. *Hydrometallurgy* **2019**, *187*, 149–157. [[CrossRef](#)]
11. Ilankoon, I.M.S.K.; Neethling, S.J. The Effect of Particle Porosity on Liquid Holdup in Heap Leaching. *Miner. Eng.* **2013**, *45*, 73–80. [[CrossRef](#)]
12. Kotsiopoulos, A.; Harrison, S.T.L. Co-Disposal of Benign Desulfurised Tailings with Sulfidic Waste Rock to Mitigate ARD Generation: Influence of Flow and Contact Surface. *Miner. Eng.* **2018**, *116*, 62–71. [[CrossRef](#)]
13. O’Kane, M.; Barbour, S.L.; Haug, M.D. A Framework for Improving the Ability to Understand and Predict the Performance of Heap Leach Piles. In Proceedings of the COPPER 99—COBRE 99 International Conference; Minerals, Metals, and Materials Society, Phoenix, AZ, USA, 10–13 October 1999; Pennsylvania State University: State College, PA, USA, 1999; Volume 4, pp. 409–419.
14. van Staden, P.J.; Petersen, J. The Effects of Simulated Stacking Phenomena on the Percolation Leaching of Crushed Ore, Part 1: Segregation. *Miner. Eng.* **2018**, *128*, 202–214. [[CrossRef](#)]
15. Ilankoon, I.M.S.K.; Neethling, S.J. Hysteresis in Unsaturated Flow in Packed Beds and Heaps. *Miner. Eng.* **2012**, *35*, 1–8. [[CrossRef](#)]
16. Wang, L.; Yin, S.; Deng, B. Understanding the Effect of Stepwise Irrigation on Liquid Holdup and Hysteresis Behavior of Unsaturated Ore Heap. *Minerals* **2021**, *11*, 1180. [[CrossRef](#)]
17. Bouffard, S.C.; West-Sells, P.G. Hydrodynamic Behavior of Heap Leach Piles: Influence of Testing Scale and Material Properties. *Hydrometallurgy* **2009**, *98*, 136–142. [[CrossRef](#)]
18. Fagan, M.A.; Ngoma, I.E.; Chiume, R.A.; Minnaar, S.; Sederman, A.J.; Johns, M.L.; Harrison, S.T.L. MRI and Gravimetric Studies of Hydrology in Drip Irrigated Heaps and Its Effect on the Propagation of Bioleaching Micro-Organisms. *Hydrometallurgy* **2014**, *150*, 210–221. [[CrossRef](#)]
19. Chiume, R.; Minnaar, S.H.; Ngoma, I.E.; Bryan, C.G.; Harrison, S.T.L. Microbial Colonisation in Heaps for Mineral Bioleaching and the Influence of Irrigation Rate. *Miner. Eng.* **2012**, *39*, 156–164. [[CrossRef](#)]
20. de Andrade Lima, L.R.P. Liquid Axial Dispersion and Holdup in Column Leaching. *Miner. Eng.* **2006**, *19*, 37–47. [[CrossRef](#)]
21. de Klerk, A. Liquid Holdup in Packed Beds at Low Mass Flux. *AIChE J.* **2003**, *49*, 1597–1600. [[CrossRef](#)]
22. Gibb, J.; Barcelona, M.J.; Ritchey, J.D.; LeFaivre, M.H. *Effective Porosity of Geologic Materials: First Annual Report*; Illinois State Water Survey: Champaign, IL, USA, 1984.
23. Ilankoon, I.M.S.K.; Neethling, S.J. Transient Liquid Holdup and Drainage Variations in Gravity Dominated Non-Porous and Porous Packed Beds. *Chem. Eng. Sci.* **2014**, *116*, 398–405. [[CrossRef](#)]
24. Ribeiro, A.; Neto, P.; Pinho, C. Mean Porosity and Pressure Drop Measurements in Packed Beds of Monosized Spheres: Side Wall Effects. *Int. Rev. Chem. Eng.* **2010**, *2*, 40–46.
25. Wu, A.; Yin, S.; Qin, W.; Liu, J.; Qiu, G. The Effect of Preferential Flow on Extraction and Surface Morphology of Copper Sulphides during Heap Leaching. *Hydrometallurgy* **2009**, *95*, 76–81. [[CrossRef](#)]
26. Pereira, G.; Moreira, R.; Vázquez, M.J.; Chenlo, F. Kinematic Viscosity Prediction for Aqueous Solutions with Various Solutes. *Chem. Eng. J.* **2001**, *81*, 35–40. [[CrossRef](#)]
27. Basson, P.; Gericke, M.; Grewar, T.L.; Dew, D.W.; Nicol, M.J. The Effect of Sulphate Ions and Temperature on the Leaching of Pyrite. III. Bioleaching. *Hydrometallurgy* **2013**, *133*, 176–181. [[CrossRef](#)]
28. Xia, F.; Zhao, J.; Etschmann, B.E.; Brugger, J.; Garvey, C.J.; Rehm, C.; Lemmel, H.; Ilavsky, J.; Han, Y.-S.; Pring, A. Characterization of Porosity in Sulfide Ore Minerals: A USANS/SANS Study. *Am. Mineral.* **2014**, *99*, 2398–2404. [[CrossRef](#)]
29. Odidi, M.; Fagan-Endres, M.; Harrison, S.T.L.; Ngoma, E.; Petersen, J. *Equipment for Studies on Heap Leaching Test Columns*; University of Cape Town: Cape Town, South Africa, 2020. Available online: https://zivaHub.uct.ac.za/articles/Equipment_for_Studies_on_Heap_Leaching_Test_Columns/11907027/2 (accessed on 7 February 2023).
30. Bouffard, S.C. Review of agglomeration practice and fundamentals in heap leaching. *Miner. Process. Extr. Metall. Rev.* **2005**, *26*, 233–294. [[CrossRef](#)]
31. Macías-García, A.; Cuerda-Correa, E.M.; Díaz-Díez, M.A. Application of the Rosin–Rammler and Gates–Gaudin–Schuhmann Models to the Particle Size Distribution Analysis of Agglomerated Cork. *Mater. Charact.* **2004**, *52*, 159–164. [[CrossRef](#)]
32. Vítěz, T.; Trávníček, P. Particle Size Distribution of a Waste Sand from a Waste Water Treatment Plant with Use of Rosin–Rammler and Gates–Gaudin–Schuhmann Mathematical Model. *Acta Univ. Agric. Silvic. Mendel. Brun.* **2014**, *59*, 197–202. [[CrossRef](#)]
33. Fagan-Endres, M.A.; Odidi, M.D.; Harrison, S.T.L. An Accurate Residence Time Distribution Measurement Method for Low Volumetric Flowrate Systems, with Application to Heap Leaching Columns. *Chem. Eng. Commun.* **2023**, *210*, 1–7. [[CrossRef](#)]
34. Wu, A.; Yang, B.; Xi, Y.; Jiang, H. Pore Structure of Ore Granular Media by Computerized Tomography Image Processing. *J. Cent. South Univ. Technol.* **2007**, *14*, 220–224. [[CrossRef](#)]
35. Ilankoon, I.M.S.K.; Neethling, S.J. Liquid Spread Mechanisms in Packed Beds and Heaps. The Separation of Length and Time Scales Due to Particle Porosity. *Miner. Eng.* **2016**, *86*, 130–139. [[CrossRef](#)]

36. Yin, S.; Wang, L.; Chen, X.; Wu, A. Effect of Ore Size and Heap Porosity on Capillary Process inside Leaching Heap. *Trans. Nonferrous Met. Soc. China* **2016**, *26*, 835–841. [[CrossRef](#)]
37. Odidi, M.D.; Fagan-Endres, M.A.; Harrison, S.T.L. Moisture Absorption Rates via Capillary Suction within Packed Beds—The Effect of Material and Fluid Properties with Implications for Heap Leaching Operations. *Hydrometallurgy* **2023**, *215*, 105975. [[CrossRef](#)]

Disclaimer/Publisher’s Note: The statements, opinions and data contained in all publications are solely those of the individual author(s) and contributor(s) and not of MDPI and/or the editor(s). MDPI and/or the editor(s) disclaim responsibility for any injury to people or property resulting from any ideas, methods, instructions or products referred to in the content.